THE ASTROPHYSICAL JOURNAL, 467:227–240, 1996 August 10

OBSERVATIONS AND MODELING OF THE NUCLEAR STARBURST IN NGC 6946[1]

C. W. ENGELBRACHT, M. J. RIEKE, AND G. H. RIEKE
Steward Observatory, University of Arizona, Tucson, AZ 85721

AND

WILLIAM B. LATTER[2]
National Radio Astronomy Observatory,[3] 949 N. Cherry Avenue, Tucson, AZ 85721
Received 1995 December 8; accepted 1996 February 29

ABSTRACT

Near-infrared images in both broad and narrow bands, plus long-slit and aperture spectroscopy at moderate and high resolution have been obtained for NGC 6946. We have used these data and data from the literature to derive a set of observational constraints on the stellar population in the nucleus.

We estimate an ultraviolet flux of 10^{52} ionizing photons s^{-1}. A thorough examination of the gas and stellar motions puts a 2 σ upper limit on the dynamical mass in the central 8″.5 (which corresponds to 230 pc at an assumed distance of 5.5 Mpc) of $\sim 3 \times 10^8$ $M_\odot$. A detailed study of broadband colors, emission-line ratios, and the 10 μm silicate absorption feature indicates that the extinction to the starburst is high, with $A_V = 10.4$ mag. An estimate of the supernova rate from both nonthermal radio emission and [Fe II] 1.644 μm emission from gas excited in fast shocks agrees well with our models. The current rate of supernova explosions in the nucleus is $\sim 6 \times 10^{-3}$ yr^{-1}. The bolometric luminosity of the starburst region is greater than 2.2×10^9 $L_\odot$.

In addition to the diagnostic features we have used here, the infrared spectra show a wealth of stellar features and weaker emission lines, including atomic absorption lines and several H_2 emission lines. We have measured the lines of H_2 and compared the ratios to models to determine the excitation mechanism.

The properties of NGC 6946 have been fitted with a starburst model. We find that the starburst probably had a duration of ~ 20 million years and that the star formation is likely to be biased toward high-mass stars compared with those in the local neighborhood.

Subject headings: galaxies: individual (NGC 6946) — galaxies: photometry — galaxies: starburst — infrared: galaxies

1. INTRODUCTION

A significant fraction of nearby galaxies have strong, centrally concentrated infrared sources indicative of rapid star formation in their central few hundred parsecs (Rieke & Lebofsky 1978; Devereux, Becklin, & Scoville 1987). Detailed studies of these nuclear starbursts have concentrated on cases of moderate (e.g., Rieke et al. 1980, 1993; Krabbe, Sternberg, & Genzel 1994), or high (e.g., Rieke & Lebofsky 1985; Goldader et al. 1995) luminosity. It is likely that most of the well-studied starbursts are also relatively young, since such systems are the most dramatic and hence will tend to stand out in surveys. An understanding of how these events occur and evolve will require study over the full range of scale and age. To this end, we report a detailed study of the starburst in the nucleus of NGC 6946, which is an order of magnitude less luminous than the moderate events that are the subject of previous work.

Large amounts of dust and accompanying extinction appear to be common among young starbursts, hindering optical observations. Observations of the stellar population are easier to interpret in the near-infrared where extinction is only about 10% of that in the optical. Far-infrared emission of starlight reradiated by dust and radio flux from supernova remnants put important constraints on the starburst population, but the near-infrared spectral region offers the only direct glimpse of the integrated stellar population in the burst.

Advances in infrared spectrometers will allow us to obtain high-resolution (~ 100 km s^{-1}), near-infrared spectra of starbursts, with high signal-to-noise ratios. We report one of the first such spectra. In addition to providing observations of many stellar absorptions and a number of nebular emission lines in NGC 6946, this spectrum allows us to determine the dynamical mass in the starburst region. The new constraints derived from this spectrum and accompanying images are combined with information from the literature and compared with a suite of starburst models to determine the age of the event and to constrain the initial mass function and time history of star formation.

2. OBSERVATIONS AND DATA REDUCTION

2.1. *Imaging*

Broadband images of NGC 6946 in the *J*, *H*, and *Ks* bands were obtained on 1994 June 21 at the Steward Observatory Bok 2.3 m telescope on Kitt Peak with a NICMOS 3–based camera. Images of the galaxy were interleaved with blank sky observations, and both on- and off-source frames were jittered by several arcseconds on the sky so that bad pixels would be removed in a median combination of the images. Temporally adjacent sky images were subtracted from each galaxy frame, and the sky images were median-combined and dark-current–subtracted to

[1] Observations reported in this paper were obtained with the Multiple Mirror Telescope operated by the Smithsonian Astrophysical Observatory and the University of Arizona.

[2] Current address: NASA/Ames Research Center, Mail Stop 245-3, Moffett Field, CA 94035.

[3] NRAO is operated by Associated Universities, Inc., under cooperative agreement with the National Science Foundation.

make a flat field, which was divided into the object frames. The object frames in each filter were aligned using field stars in the frame for reference and were then median-combined to produce images with a total integration time of 2–3 minutes. The final frames at H and Ks were magnified by small factors (1.011 at H and 1.014 at Ks) so that the scales matched the images taken at J. The frames were aligned to a common center using the many stars in the field for reference. The final frames are presented as gray-scale plots in Figure 1 at a scale of 0.″62 pixel^{-1}.

The broadband images were calibrated by scaling them to match the flux in a 27.″4 aperture measured by Aaronson (1977). The image taken through the Ks filter was scaled to match Aaronson's K-band photometry, so we will hereafter refer to this image as the K-band image. Aaronson's apertures are overlaid on the K-band contour map in Figure 1. Measurements from this paper are compared to Aaronson's photometry in Table 1. The agreement is good except for the largest aperture, in which Aaronson had to correct for a star in the reference beam. We therefore take our photometric errors to be the same as those of Aaronson, i.e., 0.06, 0.05, and 0.03 mag at J, H, and K, respectively. The seeing as measured from the many stars in the field is approximately 1.″2 FWHM.

The narrowband images were acquired with the same instrumentation and ~0.5% bandwidth filters on 1993 October 27. The filters were tuned by tilting to hydrogen Brγ ($\lambda = 2.1655$ μm), H_2 $v = 1 \rightarrow 0$ $S(1)$ ($\lambda = 2.1213$ μm), and adjacent continuum (see Latter et al. 1993 for details).

TABLE 1

APERTURE PHOTOMETRY OF NGC 6946 AT J, H, AND K

APERTURE (arcseconds)	THIS PAPER			AARONSON 1977		
	$J-H$	$H-K$	m_K	$J-H$	$H-K$	m_K
3	0.86	0.55	10.66	...	...	...
8.5	1.02	0.47	9.44	...	...	...
27.4	0.96	0.39	8.62	0.96	0.39	8.62
41.1	0.92	0.39	8.29	0.94	0.37	8.29
105	0.75	0.46	7.49	0.96	0.34	7.22

NOTE.—The photometry presented here and the Aaronson 1977 photometry were set equal in the 27.″4 aperture.

Several techniques for continuum subtraction were used, each giving similar results. The narrowband images were magnified by a factor of 0.98 to match the scale of the broadband images and were aligned with the broadband images using the many stars in the field. The central 10″ of these images is presented as gray-scale and contour plots in Figure 2.

2.2. *Spectroscopy*

2.2.1. *J-Band Spectroscopy*

The J-band spectra were obtained at the Multiple Mirror Telescope (MMT) on 1993 October 2, using GeSpec, a germanium diode spectrometer. The array consists of two rows of 32 elements each, one for sky and one for the object, corresponding to a spectral coverage of about 0.023 μm per

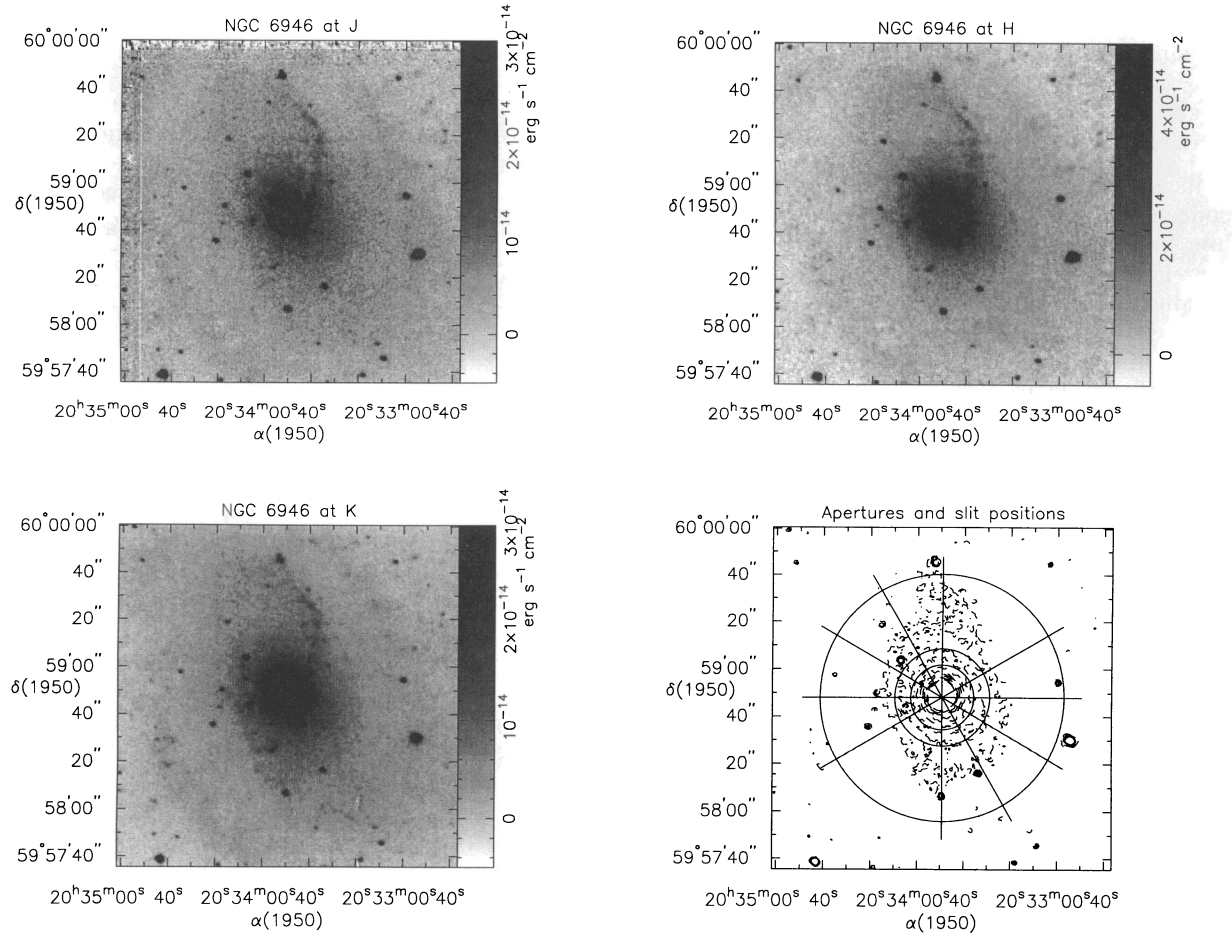

FIG. 1.—Gray-scale images of NGC 6946 at J (*top left*), H (*top right*), and K (*bottom left*), plus a contour map at K (*bottom right*) overlaid with the slit positions and photometry apertures. The straight lines in the last panel indicate the length and positions of the slit, which was 2.″4 wide.

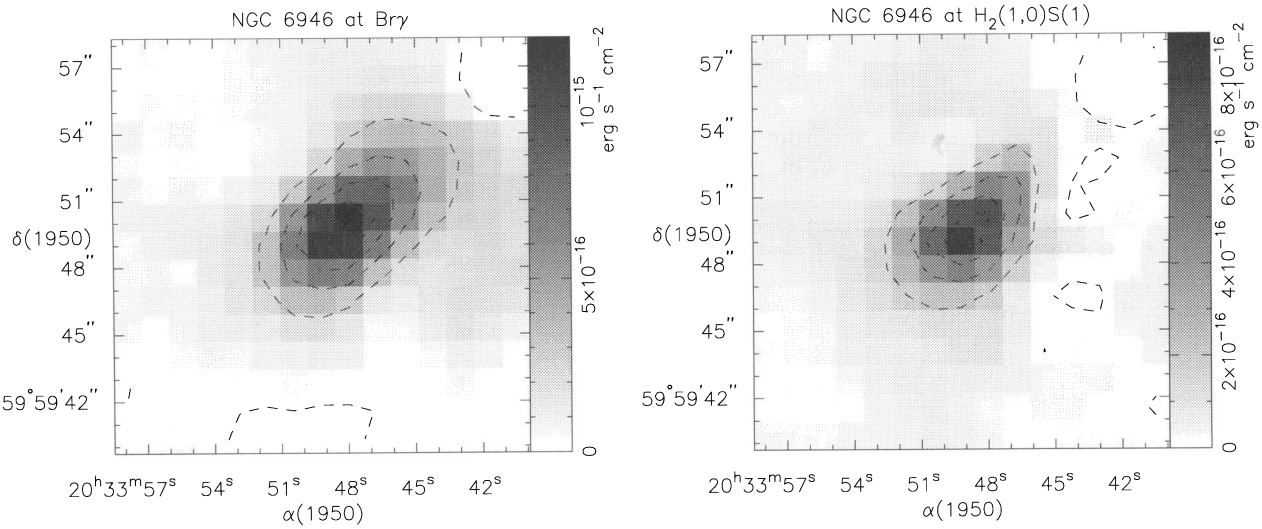

FIG. 2.—Gray-scale and contour plots of the central 10″ of NGC 6946 in narrowband filters tuned to H_2 (2.121 μm), displayed on the right, and Brγ (2.166 μm), displayed on the left.

grating setting at our resolution ($\lambda/\Delta\lambda \sim 800$). The instrument and observing techniques are described in Rix et al. (1990). The data are presented in Figure 3. We used five grating settings chosen to include important lines. We used a more nearly complete spectrum of M82 taken with this instrument (McLeod et al. 1993) to select spectral regions of interest. The spectra were corrected for atmospheric transmission variations using the nearby G3 V star HR 7783.

The spectra were initially flux calibrated by assuming blackbody emission from the standard star; a small adjustment was then made to make the spectrum consistent with our calibrated *J*-band image (see Table 1). The magnitude was converted to flux density using the zero points of Campins, Rieke, & Lebofsky (1985).

2.2.2. *H- and K-Band Spectroscopy*

The *H*- and *K*-band spectra were obtained at the Bok telescope on 1993 September 26 with FSpec, a cryogenic long-slit near-infrared spectrometer using a NICMOS 3 array (Williams et al. 1993). We used both low-resolution ($R \sim 700$) and high-resolution ($R \sim 2000$ at *H* and $R \sim 3000$ at *K*) modes at a position angle of 90°. The slit was two pixels wide, or 2″.34. We have also obtained additional data at position angles 0°, 30°, 60° (the position angle of the major axis of the galaxy; Rogstad & Shostak 1972), and 120° at the wavelengths of H_2(1, 0) *S*(1) and Brγ plus the first-overtone CO bands at 2.3 μm. Except for data at the position angle of 0°, the additional measurements were made after an improved array had been installed in FSpec and are of longer integration time and so have a higher signal-to-noise ratio than the other measurements. Figure 1 shows a graphical representation of the slit positions and lengths overlaid on the *K*-band contour map.

The *H*- and *K*-band data were reduced using IRAF routines and scripts written specifically for FSpec. From each image a background consisting of the average of the images taken before and after was subtracted. This process removed the sky background as well as the dark current. Dark-current–corrected observations of a blank screen were used to flat-field the data. In the longer galaxy exposures the background frames were rescaled slightly to improve the removal of airglow lines. The images were shifted and then median-combined to produce a final two-dimensional spectrum. The galaxy spectrum at each grating setting was then divided by the corresponding spectrum of the F5 V star HR 7727 (which had been reduced in a similar manner) to remove the effects of atmospheric absorption.

Since the spectrum of an F5 star is not completely featureless at this wavelength and resolution, the galaxy spectrum was multiplied by a high-resolution solar spectrum

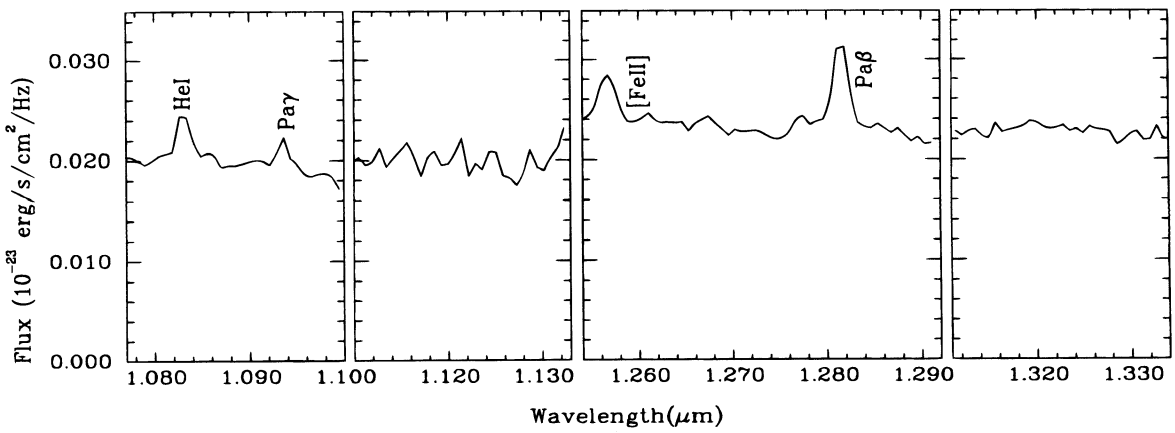

FIG. 3.—Flux-calibrated spectrum of NGC 6946 at *J* in a 3″ aperture centered on the nucleus

obtained by Livingston & Wallace (1991), convolved with a Gaussian to the same resolution as the galaxy data and normalized to a flat continuum. This procedure is described in detail by Maiolino, Rieke, & Rieke (1996). The continuum slope of the standard star was removed from the final galaxy spectrum by multiplying the spectrum by that of a blackbody at 6200 K.

The segments of corrected galaxy spectrum were wavelength calibrated using the wavelengths of OH airglow lines tabulated in Oliva & Origlia (1992). For the grating setting centered at 2.35 μm where the OH features are weak, we obtained a wavelength solution from a Ne-Kr lamp. This solution was confirmed by comparing the regions of overlap with the 2.28 μm observations and by the wavelengths of the first-overtone CO bands in the galaxy spectra.

The spectra were flux calibrated from the broadband images, using the absolute calibration of Campins et al. (1985). The spectra are displayed in Figures 4 and 5, with individual feature measurements in Tables 2, 3, 4, 5, and 6. The quality of the spectra is evident from the many detected stellar absorptions. These features are narrow; the velocity dispersion in the nucleus of NGC 6946 is very low, as discussed in § 3.8.1. The complicated continuum structure gives rise to some uncertainty in the line measurements. The

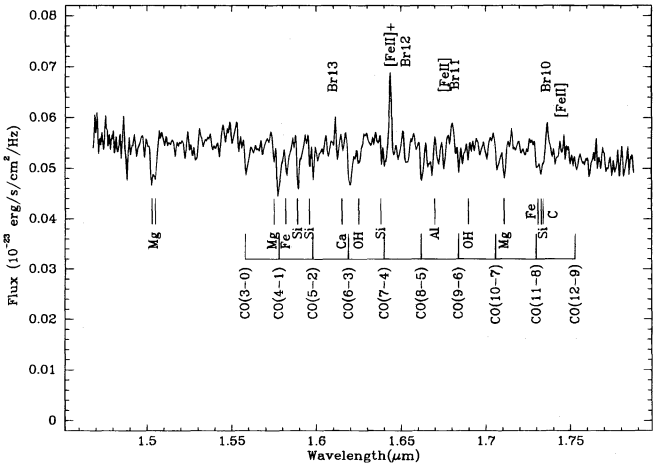

FIG. 4.—Flux-calibrated spectrum of NGC 6946 at H; the slit is oriented east-west and is 2.″4 wide. The spectrum is 12″ along the slit.

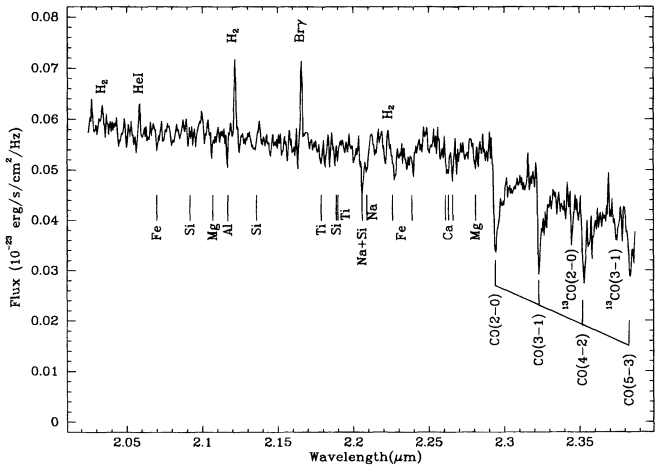

FIG. 5.—Flux-calibrated spectrum of NGC 6946 at K. Details as for the H-band spectrum.

TABLE 2

HYDROGEN RECOMBINATION LINE MEASUREMENTS

Line	λ (μm)	Flux (ergs s^{-1} cm^{-2})	Beam (arcseconds)	Source
Paβ ...	1.282	$3.0 \pm 0.4 \times 10^{-14}$	3.0	Spectra
Paγ	1.094	$1.0 \pm 0.1 \times 10^{-14}$	3.0	Spectra
Brα	4.051	$2.3 \pm 0.2 \times 10^{-13}$	7.2	Ho et al. (1990)
Brγ	2.166	$7.9 \pm 0.8 \times 10^{-14}$	7.2	Ho et al. (1990)
Brγ	2.166	$2.9 \pm 0.3 \times 10^{-14}$	8.5	NB image
Brγ	2.166	$2.6 \pm 0.3 \times 10^{-14}$	7.2	NB image
Brγ	2.166	$2.3 \pm 0.2 \times 10^{-14}$	5.9	NB image
Brγ	2.166	$1.3 \pm 0.1 \times 10^{-14}$	3.0	NB image
Brγ	2.166	$1.7 \pm 0.2 \times 10^{-14}$	2.4 × 8.5	NB image
Brγ	2.166	$1.5 \pm 0.2 \times 10^{-14}$	2.4 × 8.5 (E-W)	Spectra
Brγ	2.166	$1.8 \pm 0.2 \times 10^{-14}$	2.4 × 8.5 (N-S)	Spectra
Br10...	1.736	$3.4 \pm 1.0 \times 10^{-15}$	2.4 × 8.5 (E-W)	Spectra
Br11...	1.681	$3.7 \pm 1.5 \times 10^{-15}$	2.4 × 8.5 (E-W)	Spectra
Br13...	1.611	$3.4 \pm 1.1 \times 10^{-15}$	2.4 × 8.5 (E-W)	Spectra

NOTE.—Br12 was not measured because it is blended with the 1.644 μm [Fe II] line.

TABLE 3

[FE II] EMISSION

λ (μm)	Flux (ergs s^{-1} cm^{-2})	Beam (arcseconds)
1.257.....	$1.7 \pm 0.2 \times 10^{-14}$	3.0
1.321.....	$<10^{-15}$	3.0
1.328.....	$<10^{-15}$	3.0
1.533.....	$<10^{-15}$	2.4 × 8.5 slit
1.599.....	?	2.4 × 8.5 slit[a]
1.644.....	$2.7 \pm 0.4 \times 10^{-14}$	2.4 × 8.5 slit[b]
1.644.....	$2.1 \pm 0.3 \times 10^{-14}$	3.0[b,c]
1.644.....	$4.6 \pm 0.7 \times 10^{-14}$	8.5[b,c]
1.677.....	$2.1 \pm 2.0 \times 10^{-15}$	2.4 × 8.5 slit

[a] Value is uncertain because the line is completely blended with ^{12}CO(5, 2).

[b] Flux in this line has been corrected for stellar absorption and hydrogen emission as described in the text.

[c] Corrections to these apertures have been determined by assuming that the [Fe II] emission is distributed similarly to Brγ.

TABLE 4

HE EMISSION-LINE STRENGTHS

λ (μm)	Flux (ergs s^{-1} cm^{-2})
1.083.....	$2.0 \pm 0.3 \times 10^{-14}$
2.058.....	$2.2 \pm 0.9 \times 10^{-15}$

TABLE 5

H_2 LINE STRENGTH RELATIVE TO $H_2(1, 0)$ $S(1)$

Transition	λ (μm)	Observed Ratio	Pure Fluorescence	Thermal
(5, 3) $Q(1)$.....	1.493	<0.08	0.43	1×10^{-4}
(4, 2) $O(3)$.....	1.510	<0.08	0.42	7×10^{-4}
(6, 4) $Q(1)$.....	1.601	<0.08	0.33	1×10^{-5}
(5, 3) $O(3)$.....	1.613	<0.08	0.38	9×10^{-5}
(6, 4) $O(3)$.....	1.732	<0.08	0.31	1×10^{-5}
(1, 0) $S(2)$	2.033	0.17 ± 0.04	0.50	0.37
(2, 1) $S(3)$	2.073	~0.08	0.35	0.08
(1, 0) $S(1)$	2.121	1.00	1.00	1.00
(2, 1) $S(2)$	2.154	<0.08	0.28	0.03
(1, 0) $S(0)$	2.223	0.20	0.46	0.21
(2, 1) $S(1)$	2.247	~0.08	0.56	0.08

NOTE.—$H_2(1, 0)$ $S(1)$ flux: $1.2 \pm 0.1 \times 10^{-14}$ ergs s^{-1} cm^{-2}.

TABLE 6

ABSORPTION FEATURES

Species	λ (μm)	W_λ (Å)
Mg I	1.504	6.0
^{12}CO(3, 0).....	1.559	4.5
^{12}CO(4, 1).....	1.578	6.7
Fe I	1.583	3.3
Si I	1.590	3.7
^{12}CO(6, 3).....	1.620	5.5
^{12}CO(8, 5).....	1.663	3.1
Fe I	2.070	1.8
Mg I	2.107	1.9
Al I	2.117	1.4
Ti I.....	2.179	2.3
Na I.....	2.207	8.2
Fe I	2.227	4.4
Ca I.....	2.263	4.1
Ca I.....	2.266	3.2
^{12}CO(2, 0).....	2.296	14.6
^{12}CO(3, 1).....	2.325	17.0
^{13}CO(2, 0).....	2.346	13.3
^{12}CO(4, 2).....	2.352	15.7
^{13}CO(3, 1).....	2.374	19.5

errors in the emission-line measurements were estimated by testing a range of plausible continuum placements. The errors on the narrowband imaging measurements were obtained by assuming that the calibration is good to within 10%.

3. DISCUSSION

The distance to NGC 6946 is uncertain; estimates from 4 to 11 Mpc are in the literature. For this work we will take the distance to be 5.5 Mpc (Tully 1988), which is a conservative estimate as far as our model predictions are concerned. Adopting a larger distance would increase luminosities and make the inferred starburst more powerful. We also adopt a reference aperture of 8.″5 (which corresponds to a linear distance of 230 pc at the assumed distance to the galaxy) in which to derive the starburst properties; this aperture contains nearly all the 10 μm flux (Telesco, Dressel, & Wolstencroft 1993) and most of the Brγ flux, as shown by the narrowband images presented here.

3.1. *Morphology*

NGC 6946 is a nearly face-on (inclination 31°) Scd galaxy with a well-defined spiral pattern (Elmegreen, Meloy Elmegreen, & Montenegro 1992). The northern arm is very prominent near the nucleus in both broadband optical and Hα images, in CO(1 → 0) (Ishizuki et al. 1990), and in our broadband infrared images. It can be seen from Table 1 that the infrared colors grow systematically redder with decreasing aperture, with $H-K \sim 0.55$ on the nucleus. A map of the $H-K$ color in Figure 6 also shows that the red colors extend to the north along the prominent spiral arm. If we assume that these colors result from extinction and hence trace dust and molecular gas, our observations extend the argument of Ishizuki et al. (1990) that the gas flows to the nucleus mainly along this spiral arm. The $J-H$ color map shows similar structure but its morphology is considerably more complex than the $H-K$ image, probably due to patchy dust extinction which shows up at a stronger level at shorter wavelengths.

3.2. *Extinction*

We can estimate the extinction to the stars using our broadband colors and assuming an intrinsic color for the stellar population: the $H-K$ color is typically 0.2 mag throughout the entire Hubble sequence, while a typical $J-H$ color is 0.7 mag (Aaronson 1977). Our starburst models match these colors within a few million years after the burst, so we believe these are appropriate values to apply to NGC 6946. We derive color excesses in an 8.″5 aperture of $E(H-K) = 0.27$ and $E(J-H) = 0.32$ from the measurements in Table 1. Using the extinction law of Rieke & Lebofsky (1985), a simple foreground screen model for the dust indicates $A_V = 3.0$ mag from the $J-H$ color and $A_V = 4.3$ mag from the $H-K$ color. A small fraction of that extinction ($\sim$0.1 mag in the K band) is due to dust in our own Galaxy. Throughout this section we will include the Galactic extinction in our estimates of the total extinction, regardless of dust geometry.

The extinction derived from the $H-K$ color must be considered an upper limit if there is significant contribution to the K-band emission by hot dust or some other nonstellar source. If dust were filling in the red end of the K

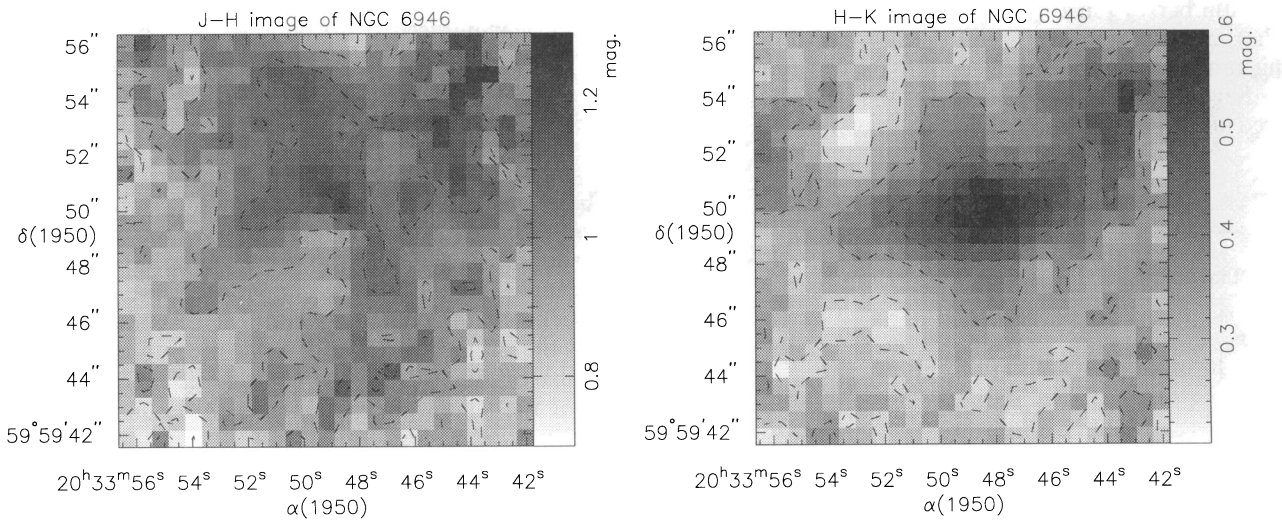

FIG. 6.—$J-H$ and $H-K$ color maps of the nuclear region. $J-H$ is on the left and $H-K$ is on the right. Both images are centered on the K-band emission peak.

band, however, the first-overtone CO bands at $\lambda = 2.3$ μm would appear weakened relative to the second-overtone bands around $\lambda = 1.6$ μm. Since the relative strengths of the first- and second-overtone CO bands in NGC 6946 fall well within the scatter of Galactic supergiant values (Origlia, Moorwood, & Oliva 1993), emission by dust in the K band must be negligible.

The dust extinction models of Witt, Thronson, & Capuano (1992) include scattering effects and dust distributions mixed with the stars, and hence are more realistic than a foreground screen model. Our $J-H$ and $H-K$ colors most closely match their starburst model, with 10.4 mag of extinction at V. The effective extinctions in the near-infrared bands indicated by the Witt et al. model are $A_J = 1.21$, $A_H = 0.75$, and $A_K = 0.48$ mag. As it happens, these are exactly the same values derived from the foreground screen model with $A_V = 4.3$ using just the $H-K$ color.

The extinction to the gas can be estimated from the hydrogen and [Fe II] lines, as summarized in Table 7. The observed hydrogen recombination ratios agree well with case B ratios reddened by the same amount as the stellar continuum. Br12 (1.64 μm) was excluded from this comparison because it is blended with the 1.644 μm [Fe II] line. The [Fe II] (1.257 μm) and [Fe II] (1.644 μm) lines share the same upper level, so their emissivities can be related simply by

$$\frac{j_{ik}}{j_{im}} = \frac{A_{ik}}{A_{im}} \frac{\lambda_{im}}{\lambda_{ik}} . \quad (1)$$

Using the transition probabilities of Nussbaumer & Storey (1988), the intrinsic ratio of the 1.644 μm line to the 1.257 μm line is 0.74. The observed ratio (where we have corrected the 1.644 μm flux as described in § 5.1) is 1.2, also in satisfactory agreement with the value of 1.0 derived from the continuum reddening estimate.

Since the near-IR extinction is insensitive to the dust geometry (in the models considered here), we will correct the continuum and line emission for a foreground screen of $A_V = 4.3$, using the Rieke & Lebofsky (1985) extinction law and interpolating as necessary to the appropriate wavelengths.

3.3. *UV Flux*

The number of ionizing photons per second, $N_{\rm Lyc}$, and the characteristic temperature of the UV-emitting stars are strong functions of the number and spectral types of hot stars. Several emission features in the near- and mid-infrared allow us to estimate these parameters.

TABLE 7

LINE RATIOS WITH REDDENING

Line Ratio	Predicted Value[a]	Reddened Value[b]	Observed Value
Paβ/Paγ	1.86	2.5	3.0 ± 0.5
Brγ/Paβ	0.18	0.33	0.4 ± 0.07
Brγ/Br10	3.14	3.7	5.0 ± 1.6
Brγ/Br11	4.42	5.4	4.6 ± 1.9
Brγ/Br13	7.08	9.1	5.0 ± 1.7
[Fe II] $\frac{\lambda 1.644\ \mu m}{\lambda 1.257\ \mu m}$	0.74	1.0	1.2 ± 0.2

[a] From Hummer & Storey 1987 for H, assuming $T_e = 5000$ K and $N_e = 100$ cm^{-3}; using transition probabilities from Nussbaumer & Storey 1988 for [Fe II].

[b] These line ratios were reddened with the extinction derived in § 3.2.

From the absence of the fine-structure lines [Ar III] (9.0 μm) and [Si IV] (10.5 μm) in NGC 6946, Roche et al. (1991) conclude that the temperature of the hottest stars is $\lesssim$35,000 K. At our assumed distance, they would find $N_{\rm Lyc} \sim 1.5 \times 10^{52}$ s^{-1} within a 5.″9 beam, from the strength of the [Ne II] flux and assuming solar metallicity.

We can also derive the ionization rate using the infrared hydrogen recombination line measurements from Table 2. The intensity ratios of the near-infrared recombination lines are not very sensitive to temperature and even less so to density, so here we simply use the $T_e = 5000$ K and $N_e = 10^2$ cm^{-3} derived for M82 by McLeod et al. (1993). Using an extinction-corrected Brγ flux from our narrowband image and an assumed distance of 5.5 Mpc, the recombination line ratio $I(\mathrm{H}\beta)/I(\mathrm{Br}\gamma) = 30.3$ from Hummer & Storey (1987) plus a ratio $\alpha_B/\alpha_{\mathrm{H}\beta}^{\mathrm{eff}} = 8.40$, we calculate 8.2×10^{51} ionizing photons s^{-1}, in the same 5.9″ beam used by Roche et al. Given the uncertainties involved, the results seem consistent.

Our measurement of Brγ is about 3 times fainter than that of Ho, Beck, & Turner (1990). Our data are more extensive, of higher resolution, and have a larger signal-to-noise ratio than theirs. In addition, our spectra and Brγ image were calibrated independently and give consistent results. We therefore take the Brγ flux from our data alone, obtaining 2.9×10^{-14} ergs s^{-1} cm^{-2} in a 8.″5 aperture, with a corresponding $N_{\rm Lyc}$ of 1.0×10^{52} s^{-1}. This is consistent with the estimate by Turner & Ho (1983) of 1.2×10^{52} s^{-1} from radio continuum measurements (after we correct their distance from 7.1 to 5.5 Mpc).

For our models, we adopt $N_{\rm Lyc} = 1 \times 10^{52}$ s^{-1}. This estimate of $N_{\rm Lyc}$ ignores the absorption of potentially ionizing photons by dust, with reradiation as far-infrared photons, not as recombination lines. Our models are therefore conservative in the amount of UV they require.

3.4. *Luminosity*

To estimate the total luminosity of the nuclear starburst, we have proceeded as follows. Engargiola (1991) discusses the far-infrared data and derives a luminosity within a 45″ beam (and corrected by us to a distance of 5.5 Mpc) of 2.2×10^9 $L_\odot$ for this spectral component. Using our near-infrared data and the optical measurements of Engargiola (1991, and references therein) we calculate that the optical and near-infrared contribute another 1.2×10^9 $L_\odot$ to the total in a 45″ beam.

To apply these numbers to the central 8.″5, we have compared the ground-based Q-band (21 μm) measure of Lebofsky & Rieke (1979) in a 5.″7 beam with the *IRAS* band 2 measure in a 45″ × 4′ beam. The ground-based flux has been corrected to 25 μm using the slope fitted between *IRAS* bands 2 and 3 integrated over the entire galaxy. The ground-based measure has also been corrected to an 8.″5 beam using the observed aperture dependence at 10 μm (Rieke 1976). The comparison demonstrates that virtually all the 25 μm flux in a 45″ beam centered on the nucleus must originate from the central 8.″5. We therefore derive that the far-infrared luminosity of the nuclear starburst is 2.2×10^9 $L_\odot$.

To estimate the contribution of the optical and near-infrared light to the total, we must take into account that this radiation is not distributed in the same fashion as the far-infrared flux. Using the aperture dependence of our near-infrared images as a guide, we estimate that the central

8″.5 of NGC 6946 contains 35% of the optical and near-infrared flux found in a 45″ beam. Therefore, the optical and near-infrared bands must contribute $4 \times 10^8\ L_\odot$ to the bolometric luminosity in the central 8″.5. For the starburst population, then, we derive $L_{\rm Bol} = 2.6 \times 10^9\ L_\odot$.

To estimate what contribution the preexisting stellar population in the nucleus might make to the observed fluxes, we have compared the K magnitude as a function of aperture in M31 to the mass in the same aperture. We used the K-band measurements of Aaronson (1977) and the mass determination of Tenjes, Haud, & Einasto (1994). We have assumed that M/L_K is the same in the preexisting nuclear population of NGC 6946 and in the nucleus of M31 and calculated a K magnitude for the underlying nuclear population in NGC 6946 based on our mass estimate of the old population from § 3.8 and setting the total available mass at the 2 σ upper limit derived there. Allocating $2.4 \times 10^8\ M_\odot$ to the old stellar population results in an absolute K magnitude of -17.9 for this component. This is almost exactly the same mass-to-light ratio calculated by Thronson & Greenhouse (1988) for the solar neighborhood. At the adopted distance of 5.5 Mpc, this provides roughly 20% of the broadband K-band flux, so we will subtract this amount from the observed K-band flux when we calculate the target K-band luminosity of the starburst.

The underlying stellar population also contributes no more than 15% to the bolometric luminosity. If we assume a BC_K for a K giant population of ~ 2.7 (Frogel & Whitford 1987), and $M_{\rm Bol}(\odot) = 4.75$, then the underlying nuclear population has a bolometric luminosity of roughly $4 \times 10^8\ L_\odot$, so we subtract this amount from $L_{\rm Bol}$ when we determine the target value for the starburst.

If we use our calculated number for the dynamical mass rather than the 2 σ upper limit, the contribution of the underlying population to the K-band and bolometric luminosities drops by $\frac{2}{3}$, raising the target values for the starburst but also making a corresponding reduction in the amount of mass available for the stars which generate that luminosity. The requirements for starburst models therefore become significantly more difficult.

3.5. He *Emission Lines*

We observe two fairly weak He emission lines in the spectra presented here, one at 1.083 μm and another at 2.058 μm. The fluxes in these lines are presented in Table 4. The ratio of He I (2.058 μm) to Brγ in NGC 6946 is 0.13 ± 0.06, which is small compared to the well-studied starburst M82, where the ratio is 0.43 (our unpublished data). The weakness of the He emission may indicate that the ionizing spectrum in NGC 6946 is very soft, which is consistent with the lack of high-ionization lines in the mid-infrared spectrum of Roche et al. (1991). There are complications in the interpretation of these lines, however (see, e.g., Clegg 1987; Shields 1993), and since they do not offer a strong constraint on our models we will not discuss them further here.

3.6. *Supernova Rate*

There are two independent means by which we can calculate the supernova rate. One is to assume that all the nonthermal radio flux is due to synchrotron emission from relativistic electrons accelerated in fast shocks associated with the supernovae. Ho et al. (1990) find the nonthermal portion of the 5 GHz flux to be 30 mJy in an 8″.5 aperture centered on the nucleus. At a distance of 5.5 Mpc, this corresponds to a 5 GHz luminosity of 1.1×10^{20} W Hz^{-1}. Using equation (8) of Condon & Yin (1990), which is based on observations of Galactic supernovae, we derive a supernova rate of 3×10^{-3} yr^{-1} for the nuclear region. We derive essentially the same supernova rate using the relation presented by Huang et al. (1994), which is based on observations of supernovae in M82.

[Fe II] emission is commonly observed in starburst galaxies (Moorwood & Oliva 1988). The emission is much stronger than is typical of a photoionized region, where the Fe^+ abundance is low. The Fe^+ abundance can be enhanced, however, in regions behind moderately fast ($\gtrsim 50$ km s^{-1}) shocks, as grains are destroyed and return Fe to the gas phase. The [Fe II] emission from starburst galaxies has therefore been attributed to shocks associated with supernova remnants.

The [Fe II] 1.644 μm line is blended with Br12 (1.641 μm) emission and CO(7, 4) absorption. To correct for this effect and derive an estimate of the true flux in the 1.644 μm line, we have obtained a spectrum of an M3 III star (HR 46), which matches the continuum of NGC 6946 reasonably well, and broadened its spectrum by 45 km s^{-1} (see § 3.8.1). Dividing the galaxy spectrum by the HR 46 spectrum smoothed out the absorptions in the continuum and allowed us to measure accurately the line flux. We estimated the Br12 flux to be about 3.0×10^{-15} ergs s^{-1} cm^{-2} using our Brγ measurement and the intensity ratios of Hummer & Storey (1987) and subtracted that value from the blend. The resulting [Fe II] 1.644 μm flux was corrected to the 3″ and 8″.5 apertures using the observed aperture dependence of the Brγ emission. The measured flux of this line can be found in Table 3. At 5.5 Mpc, this corresponds to a luminosity of $3.3 \pm 0.5 \times 10^{38}$ ergs s^{-1} cm^{-2} (corrected for extinction). Assuming that the average [Fe II] luminosity of a supernova remnant (SNR) in NGC 6946 is about equal to the 2×10^{36} ergs s^{-1} cm^{-2} of a galactic SNR (Moorwood & Oliva 1988) and that the luminous phase of the SNR lasts about 2×10^4 yr (Condon & Yin 1990), we derive a supernova rate of $8 \pm 1 \times 10^{-3}$ yr^{-1}. Vanzi et al. (1996) have analyzed the supernova rate and [Fe II] emission in M82. Their relation would indicate a rate of 5×10^{-3} yr^{-1} for NGC 6946.

We take the supernova rate to be the average of these results and the uncertainty to be large, i.e., $6 \pm 3 \times 10^{-3}$ yr^{-1} in the central 8″.5. This rate is roughly one-third the Galactic rate but for a region only 200 pc across.

3.7. *Absorption Features*

The quality of the infrared spectra permits us to study the wealth of stellar absorption features in NGC 6946. The most prominent absorption features in the spectra presented here are the first-overtone CO bands starting at 2.3 μm and to a lesser extent the second-overtone CO bands starting at 1.6 μm. Many atomic features are visible as well, with the strongest absorptions attributed to Si, Mg, and Ca. The equivalent widths of the strongest features are listed in Table 6.

The continuum spectrum of NGC 6946 is typical of a massive, evolved star. We can quantify this by comparing the strength of the CO and Si absorptions to the grid of stellar spectra of Origlia et al. (1993), in key features such as Si (1.59 μm), CO(6, 3) (1.62 μm), and CO(2, 0) (2.29 μm). In particular while the Si feature at 1.59 μm remains relatively

constant throughout the cool stellar types, late supergiants tend to have very strong CO absorptions. The continuum spectrum of NGC 6946 is most consistent with that of an M III giant or a K5 supergiant, not an unexpected result considering the other evidence (large UV flux, luminosity, and supernova rate) that we are viewing NGC 6946 several million years after a burst of star formation.

Cool stars display a steam feature around 1.9 μm, a very broad absorption which is not immediately evident in our spectra. The strength of this feature is quantified via a H_2O index, which we have determined by comparing the continuum near 2.09 and 2.29 μm (see Kleinmann & Hall 1985). We obtain a H_2O index of 0.07 mag after converting our spectroscopic index to a photometric index.

Similarly, we can measure a CO index to quantify the strength of the CO absorption. Our spectroscopic index is large, 0.35 mag. By comparison with Kleinmann & Hall (1985), a 0.35 mag spectroscopic CO index is equivalent to a 0.21 mag photometric CO index, and we assign a photometric uncertainty to this quantity of 0.03 mag. We correct the intrinsic CO index of the starburst population to 0.23 mag by assuming that an old stellar population with a CO index of 0.15 mag (typical of an old stellar population; see Frogel et al. 1978) contributes 20% of the observed K-band flux (see § 3.4).

3.8. *Mass*

We now estimate the mass of stars formed in the starburst. Since the starburst in NGC 6946 is confined to the nucleus, we can estimate the dynamical mass present in the nucleus of the galaxy to put an upper limit on the mass participating in the starburst. Both an exponential and an $r^{1/4}$ law profile were fitted to the K-band image in a least-squares fashion to determine whether the bulge was more likely to be supported by dispersion or rotation. The bulge was better fit (by an order of magnitude) by an $r^{1/4}$ law profile than an exponential. The azimuthally averaged disk profile (where we have made no correction for inclination) was well fitted to an exponential with a scale length of 31.″0, which is about 830 pc at a distance of 5.5 Mpc, and a central brightness of about 2% of the observed peak brightness.

3.8.1. *Stellar Motions*

Once it was determined that the luminosity profile of the bulge was appropriate to a spherical system, we fitted the bulge to a $\eta = 3$ model of Tremaine et al. (1994). The model profile was convolved with 1.″2 of seeing (determined from stars in the K-band image) and fitted to the galaxy profile along with the disk profile determined above. The best-fit model has a scale radius of 4.″3.

We also carefully checked for signs of rotation in the stellar features. Figure 7 shows the velocity offsets of the two strongest CO absorptions as a function of position along the slit for four position angles. Table 8 summarizes the steepness of the Doppler shift in each feature in km s^{-1} arcsec^{-1}, obtained by fitting a straight line to the points inside a 10″ radius (if that many were available). We examined both the CO(2,0) and the CO(3,1) features. The quoted error bars represent statistical uncertainties only. An indication of the true uncertainty can be obtained from the graphical representation of the measured points as shown in Figure 7. The two different filled markers both represent stellar CO features, so the points should match. We find that the stellar features are consistent with a flat curve at every position angle, with at most a rotation of a few km s^{-1} arcsec^{-1}, while the gas shows strong motions at nearly every position angle (see § 3.8.2).

Even in a heavily obscured region like the nucleus of NGC 6946, the velocity dispersion should be well represented by the broadening of the stellar CO absorption bands at 2.3 μm. We use this stellar feature to measure the dispersion because the gas may be affected by processes that have nothing to do with the gravitational potential (e.g., shocks, winds). We have measured the broadening of the CO feature in NGC 6946 by cross-correlating the galaxy spectrum with a template star spectrum with a similar CO index, as in Shier, Rieke, & Rieke (1994). The dispersion we obtain in this fashion is 45 km s^{-1} $\pm$ 10 km s^{-1} in the 2.″4 × 8″ aperture over which the spectra were extracted. The error bars indicate statistical errors determined via a Monte Carlo simulation and do not include systematic errors. From numerous tests with a suite of template stars, however, the systematic uncertainties are likely be of similar magnitude to the statistical errors at this dispersion (Shier 1995), so we simply combine the two errors in quadrature for a total error of 14 km s^{-1}. We derive the same velocity dispersion if we use the measurements along the minor axis of the galaxy (which have a higher signal-to-noise ratio and spectral resolution). These measurements agree with an independent analysis of the data by H.-W. Rix, who obtained 53 km s^{-1}.

The mass estimate was obtained by assuming that the nuclear mass is distributed similarly to the K-band light and integrating the model profile we fitted over the rectangular aperture of the slit (see Shier et al. 1994). At a radius of 4.″25, the enclosed mass in this model is $1.2^{+0.9}_{-0.6} \times 10^8\ M_\odot$, where the error bars are due to the uncertainty in the velocity dispersion. The mass estimate is insensitive to changes in r_s and η; the uncertainties are dominated by the uncertainty in the velocity dispersion. The mass estimate scales linearly with the distance to NGC 6946 and with the square of the velocity dispersion.

3.8.2. *Gas Motions*

In Figure 8 we present position-velocity maps of H_2 and Brγ. Points fitted at every pixel along the slit are plotted in

TABLE 8

VELOCITY GRADIENTS OF SPECTRAL FEATURES[a]

Feature	P.A. = 0°	P.A. = 30°	P.A. = 60°	P.A. = 90°	P.A. = 120°
Brγ	4.6 ± 2.8	29.8 ± 1.7	21.3 ± 1.0	10.1 ± 1.7	0.4 ± 1.1
$H_2(1, 0)\ S(1)$	20.8 ± 2.5	18.8 ± 0.8	15.2 ± 0.5	9.7 ± 1.3	1.1 ± 0.9
CO(2, 0)	...	−1.8 ± 2.7	−1.2 ± 2.0	−0.4 ± 5.3	−9.2 ± 2.2
CO(3, 1)	...	−13.8 ± 6.0	−1.3 ± 2.4	−9.0 ± 3.0	−5.0 ± 3.1

[a] In km s^{-1} arcsec^{-1}.

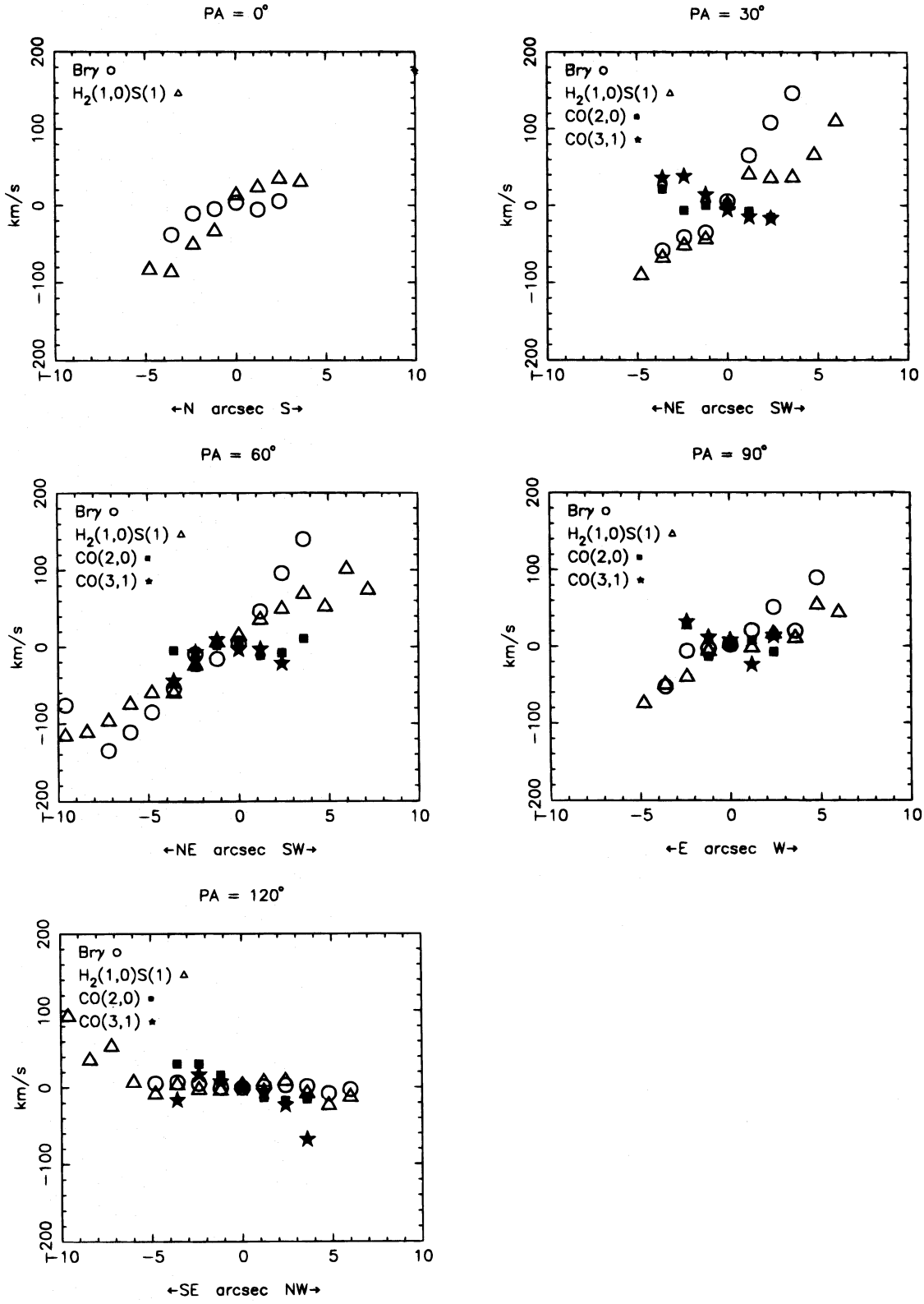

FIG. 7.—Plots of the velocity centroid offsets of stellar CO, Brγ, and H_2 at five position angles. The filled points are the stellar features, while the open markers trace gaseous features.

Figure 7, while the slope of each line in km s^{-1} $arcsec^{-1}$ as determined by a linear fit to the data points within 10″ radius is listed in Table 8. One striking result is that not only are the gas motions not consistent with the flat curves measured for the stellar features, the motions derived from lines of Brγ (from ionized gas) and H_2 (from molecular gas) are not even consistent with each other. We interpret this as evidence that the gas in the nuclear region of NGC 6946 is not a good tracer of the gravitation potential but may instead be affected by processes such as infall. In particular,

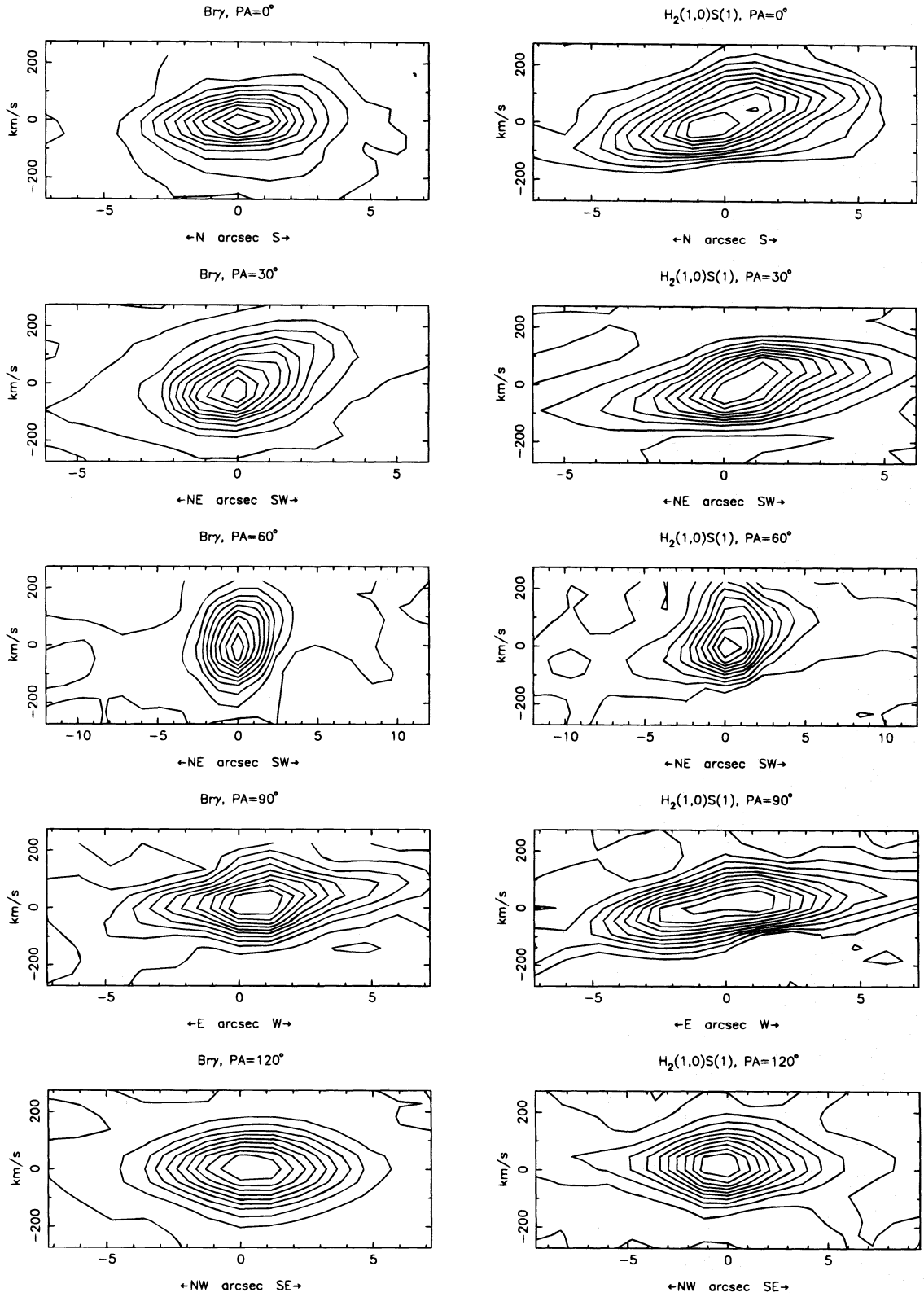

FIG. 8.—Position-velocity plots of two strong emission lines in our long-slit spectra of NGC 6946. The spatial axis is centered on the stellar continuum peak, while the velocity axis is centered on the intensity peak of the spectral line.

while Brγ at position angles of 0° and 120° (these position angles are each 30° from the minor axis of NGC 6946) and H_2 at P.A. 120° show no evidence of motion, the H_2 at 0° shows strong motion along the slit. We may be seeing some indication of the gas infall along the spiral arms observed by Ishizuki et al. (1990).

3.8.3. *Ratio of Dynamical Mass to H_2 Mass*

Some of the mass participating in the starburst must be in the form of molecular gas out of which stars are being made. Ishizuki et al. (1990) estimate that there is $\sim 3 \pm 1.5 \times 10^8$ $M_\odot$ of H_2 within a 5.″6 radius of the nucleus of NGC 6946.

We correct this value to our 4″.25 aperture by scaling by the change in disk area. This procedure may tend to underestimate the amount of molecular gas in the nucleus both because the observations show that the CO emission is strongly peaked toward the center and because any gas disk in the center is probably inclined with respect to our line of sight, but the uncertainty in the CO to H_2 conversion probably dominates any error made in this manner. Using the standard conversion, we estimate that there is $1.7 \pm 0.9 \times 10^8\ M_\odot$ of molecular gas within a 4″.25 radius of the nucleus. Although this result suggests that the ratio of molecular gas mass to dynamical mass in our 8″.5 aperture is very large, it is also likely that the conversion factor from CO to H_2 is smaller than the standard (e.g., Maloney & Black 1988).

3.8.4. *Mass Budget*

As a conservative upper limit to the dynamical mass, we take our 2 σ limit of $3 \times 10^8\ M_\odot$. We allocate some of this mass to the preexisting nuclear population and some to molecular gas currently in the nucleus as described below, leaving the remainder of the mass available as stars in the burst.

McLeod et al. (1993) make a rough argument that the gas funneling into the nucleus of a galaxy could not exceed half the dynamical mass without triggering the starburst. Bekki (1995) reports smoothed hydrodynamical calculations that suggest dynamical instabilities and probable triggering of a starburst may occur when the gas exceeds ~20% of the total mass in a strongly perturbed system, so McLeod et al. probably overestimated the portion of material that can take part in the starburst by a factor of ~2. The threshold may be as low as 10% in noninteracting systems (e.g., Wade & Habe 1992). We therefore assume that ~80% of the dynamical mass, or $2.4 \times 10^8\ M_\odot$, is tied up in old stars in an underlying nuclear population.

The remaining $6 \times 10^7\ M_\odot$ we allocate to the molecular gas that fueled the starburst; some went into making stars in the burst while the rest remains as the molecular gas measured today. Even given a $N(H_2)/I_{CO}$ conversion factor that is too large by a factor of 5, it is likely that half of this mass is still in the form of molecular gas; that is, no more than $3 \times 10^7\ M_\odot$ of stars could have formed in the burst. Given that many of the starburst parameters we have derived here are conservative limits, we favor starburst models sufficiently efficient in their use of mass that they fall well below this upper limit.

4. MODELS

We have compiled the relevant observational constraints in Table 9. We turn now to modeling the starburst. We make use of the models of Rieke et al. (1993, hereafter RLRT93), which we describe briefly below.

4.1. *M82 Models*

RLRT93 modeled the starburst in M82 using the models of Rieke et al. (1980) with updated stellar tracks and atmospheric parameters. The starburst model uses the grid of stellar evolution tracks of Maeder (1992), which have been assigned observational parameters based on a combination of atmosphere models and empirical calibration. The starburst models use the evolutionary tracks over a range of stellar masses up to 80 $M_\odot$ and interpolate between the tracks to reduce oscillations caused by discreteness in the stellar masses. The models form stars over a short Gaussian burst (FWHM of five million years), with the number of stars in each bin determined by the initial mass function (IMF). The observational parameters are predicted as the stars evolve along theoretical tracks. Further details can be found in RLRT93.

TABLE 9

SUMMARY OF STARBURST PARAMETERS

Parameter	Value
Distance	5.5 Mpc
Mass [a]	$<6 \times 10^7\ M_\odot$
L_{Bol}	$2.2 \times 10^9\ L_\odot$
M_K	<-19.5
log N_{LyC}	>52
SNR	$6 \pm 3 \times 10^{-3}$ yr^{-1}
CO	0.23 ± 0.03

[a] This mass limit includes both molecular gas and stars actually formed in the burst.

4.2. *NGC 6946 Models*

For NGC 6946, the model values of N_{Lyc}, L_{Bol}, CO index, and K-band flux are displayed as a function of time in Figure 9. Each point along the curves presented has been divided by the observed values for NGC 6946 in Table 9, so the target value for each quantity is 1. A fit can be considered good when all curves meet the target value simultaneously. In practice, since some of the observational parameters are uncertain, we choose the point on the plot where the curves come closest to meeting the target values simultaneously.

We have attempted to match the parameters of NGC 6946 with a series of starburst models with different IMFs and SFRs. The results are displayed in Figure 9. We have shown results of fits to two different IMFs. The local IMF, represented by IMF 3 of RLRT93, requires a large amount of mass ($3.3 \times 10^7\ M_\odot$) in a single burst (model A) to meet the required K magnitude and N_{Lyc}, but the bolometric luminosity predicted by the model is a factor of 1.7 greater than observed. A better fit can be achieved with a double burst, but this requires over $6 \times 10^7\ M_\odot$ of stars to meet the constraints. Because of the large mass required, we consider these models unlikely to be compatible with the observations.

The IMF found by RLRT93 to fit the M82 observations best (their IMF 8), provides a considerably better fit to the observations. This model is very efficient with mass, so that only $1.1 \times 10^7\ M_\odot$ is required in a single-burst to produce the observed K flux. The single-burst model, however, produces too much bolometric luminosity in the region where the other constraints fit, so we have modeled a double burst in model C (see Fig. 9*c*). This double burst uses a total of $1.9 \times 10^7\ M_\odot$, with the bursts separated by 20 million years and the second burst 20% as strong as the first. A reasonable fit is achieved at 32 million years, and here the bolometric luminosity is within 30% of the target value. The supernova rate, which has not been plotted here, is also reasonably consistent with the observations.

The main constraint that excludes models using local IMFs or longer SFRs is the upper limit on the mass. If we lift this constraint and allow the models to use a larger

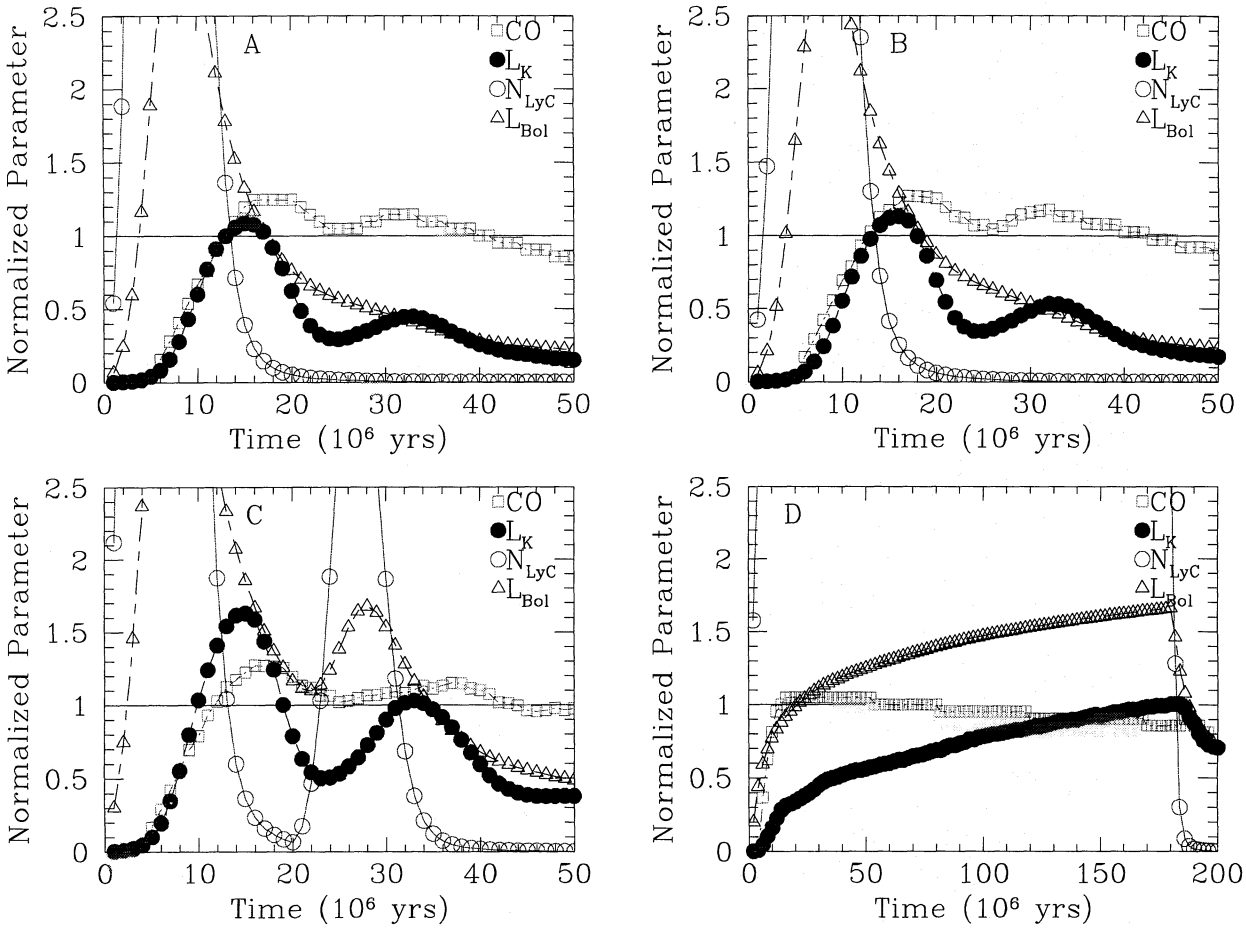

FIG. 9.—Starburst models of NGC 6946 with IMFs and SFRs as described in the text. Models A and B are single-burst models using 3.3 and 1.1 × 10^7 $M_\odot$, respectively. Model C uses a double burst with the same IMF as B and a mass in both bursts of 1.9 × 10^7 $M_\odot$. Model D forms stars at 0.56 $M_\odot$ yr^{-1} until 1.8 × 10^8 yr, at which time star formation ceases.

fraction of the dynamical mass, a burst model with an IMF biased toward massive stars is no longer required to fit the observations. For example, the double-burst, local-type IMF model described above is a reasonable fit to the observations, aside from the mass constraint.

Without the mass constraint, we can also fit models with star formation extended over a longer period of time. Models which form stars for tens of millions of years and then turn off can also match the observations, although they require most of the dynamical mass in the nucleus. One such model is model D, shown in Figure 9*d*. This model formed stars at a rate of 0.56 $M_\odot$ yr^{-1} for 1.8 × 10^8 yr using IMF 3. After the star formation shut off, N_{Lyc} and L_{Bol} dropped enough to be compatible with the observations. This model consumed 10^8 $M_\odot$ of stars. Models such as these can reasonably fit the observations (except for the mass constraint), but the star formation rate could not be maintained for more than a 100 million years or so.

It seems clear that the high rate of star formation in the nucleus of NGC 6946 must be episodic in nature rather than continuous throughout the lifetime of the galaxy. This conclusion is independent of our assumptions about the triggering of a very short burst of star formation, which presumably can only consume a small fraction of the dynamical mass in the nucleus.

If we assume that the nuclear mass is dominated by an old stellar population rather than being largely composed of new stars, our models demonstrate that a short burst of star formation with an IMF biased toward massive stars is required to match the observations of NGC 6946. Our models make use of most or all the mass we believe is available for star formation, and as such they only just meet the target *K*-band luminosity. Were we to spread the star formation over time, there would never be enough red supergiants (which produce most of the *K*-band luminosity) at any given time to meet the target luminosity. The nature of the star formation (i.e., the fact that it occurs in a burst) tightly constrains the age of the burst in the following way. The burst produces many massive stars, which produce most of the UV flux and luminosity. As these stars evolve into red supergiants, both the *K*-band luminosity and CO index of the population increase while the UV flux and total luminosity decrease rapidly. Given the requirement that the UV flux, bolometric luminosity, *K*-band luminosity, and CO index should all be quite large at the same time, the time since the last significant burst of star formation must be (within 10% or so) 7 million years, independent of which IMF is examined.

4.3. *Problems with Local IMFs*

It should be noted that our distance estimate has been conservative: several of the distance estimates to NGC 6946 are close to 10 Mpc. As we noted in § 3.8, the mass estimate scales linearly with the distance. The requirements for the

starburst model, however, depend on luminosities and hence on the square of the distance. Putting NGC 6946 at 10 Mpc would tighten the constraints and make it even more difficult to fit a local IMF to the observations.

In addition, we have ignored the absorption of Lyman continuum photons by dust, therefore reducing the requirements on the starburst models. The SFR we have chosen also makes the most efficient use of the available mass. The models presented here are therefore highly forgiving in fitting a given IMF. More realistic models would make it more difficult to fit a local IMF to the observations.

5. OTHER RESULTS

5.1. *Fe Emission*

We have examined our spectra for other [Fe II] emission lines that might be used to constrain the density in the emitting region. The measured fluxes or upper limits of these lines are presented in Table 3. Nussbaumer & Storey (1988) calculate that the ratio of [Fe II] 1.257 μm to [Fe II] 1.533 μm should be a strong function of density and plot the ratio of 1.533 μm to 1.257 μm for a range of densities from 10 cm^{-3} to 10^8 cm^{-3}. We do not directly observe the 1.533 μm line in our spectra, but we can place an upper limit on it of $\sim 10^{-15}$ ergs s^{-1} cm^{-2}, or an emissivity of about 6% of the 1.257 μm line. This limit implies a density in the emitting region of $\lesssim 2 \times 10^3$ cm^{-3}. The complicated continuum structure in the vicinity of the 1.533 μm line makes the upper limit uncertain, so we examine other [Fe II] lines to place additional constraints on the density.

There are many [Fe II] lines in the J band in addition to the 1.257 μm line. We can place upper limits on the 1.321 μm and 1.328 μm lines of 6% of the strength of the 1.257 μm line. We have calculated the ratio 1.328/1.294 μm = 0.61 using the A values of Nussbaumer & Storey (1988). This implies an upper limit for 1.294/1.257 μm of $\sim$0.1. Using the results of Hudgins, Herter, & Joyce (1990), who calculate the density dependence of the 1.294/1.257 μm ratio, this limit implies an upper limit to the density of $\lesssim 4 \times 10^3$ cm^{-3}. The strength of the 1.328 μm line is thus consistent with our low-density estimate derived from the upper limit on the 1.533 μm line.

Our failure to detect the 1.321 μm line is puzzling. This line comes from the same upper state as the 1.257 μm line, so the ratio of 1.321 μm to 1.257 μm is predicted by the A values to be 0.26. Our measured upper limit, though, puts the ratio at $\sim$0.06. At this time, we have no explanation for this anomaly unless the line falls in an absorption in the continuum spectrum.

5.2. *Molecular Hydrogen*

In many starburst galaxies, molecular hydrogen appears to be excited collisionally in regions with kinetic temperatures $T_K \gtrsim 1000$ K. Such kinetic temperatures are typically associated with moderate velocity shocks, $V_s \approx 40$–50 km s^{-1} (Draine & Roberge 1982; Hollenbach & Shull 1977). To investigate the source of the H_2 excitation in NGC 6946 we have compiled a list of observed H_2 line ratios in Table 5 and compared them to the models of Black & van Dishoeck (1987). The fluorescent line ratios were taken from their model 14, while the thermal line ratios were taken from their model S2. The H_2 emission from NGC 6946 is clearly more consistent with the Black & van Dishoeck collisional excitation model; we can place an upper limit of $\sim$15% to any optically thin fluorescent component of the 1-0 $S(1)$ line. If fluorescence plays a significant role, the emitting gas must be at high density as modeled by Sternberg & Dalgarno (1989). The importance of thermal excitation is supported indirectly by the differing velocity pattern we see in the H_2 and Brγ lines, indicating that the UV source and H_2 emission are not closely connected spatially.

6. CONCLUSIONS

We have used new infrared data and data from the literature to derive a number of properties of the nuclear starburst in NGC 6946. These include $N_{\rm Lyc}$, $L_{\rm Bol}$, absolute magnitudes in the J, H, and K bands, CO index, SNR, and the mass of stars formed in the starburst. The data were compared to starburst models to determine the age of the starburst and to put constraints on the IMF. We have taken into account the properties of a preexisting nuclear population which must underly the starburst. In deriving the starburst parameters, we have tried to be conservative in such a way that it becomes easier for a given IMF to fit the data.

We have compared our NGC 6946 data to starburst models with varying IMFs and single or double bursts of star formation. A burst of star formation converting 4×10^6 $M_\odot$ into stars occurring 7 million years ago combined with a previous burst of 1.5×10^7 $M_\odot$ 20 million years before are sufficient to account for the properties of the starburst in the nucleus of NGC 6946 if the IMF is similar to that fit to M82 by RLRT93. It is difficult to explain the observations with an IMF consistent with the local neighborhood; although the case for an IMF biased toward high masses is weaker than in the well-studied case of M82, such a bias seems likely for NGC 6946 also.

If the nuclear mass is dominated by an old stellar population, the current SFR is constrained to be a decaying burst because the limited mass available must create enough stars to produce a large K-band luminosity and a SFR with a weak time dependence never produces enough stars at a given time to meet the luminosity requirement. Regardless of the IMF we examined, the age of the burst is determined by the requirement that the starburst model simultaneously produce a large UV flux and bolometric luminosity, both of which weaken rapidly after vigorous star formation ceases, and a large CO index and K-band luminosity, which are initially weak and only become strong after the massive stars evolve into red supergiants.

We have done a detailed kinematic study of the gas and stars in the nucleus of NGC 6946. It seems clear that the processes affecting each component are different. While the stellar component shows no significant rotation and seems to be dominated by dispersion, the gas shows considerable velocity gradients across small regions of the nucleus. In particular, while the molecular gas traced by H_2 emission in our spectra seems to follow the molecular gas traced by CO emission in the radio, the ionized component we observe in Brγ shows kinematics significantly different from both the stars and the molecular gas. We suggest that in a complicated starburst region such as the nucleus of NGC 6946, it may be inappropriate to use gas as a tracer of the gravitational potential.

We have observed several transitions of [Fe II] and H_2. The former species appears to be excited in low-density regions ($\lesssim 4 \times 10^3$ cm^{-3}). The relative H_2 line strengths are inconsistent with excitation via fluorescence at moderate

densities. The emission is consistent with the thermal models of Black & van Dishoeck (1987) or with the high-density, strong UV field models of Sternberg & Dalgarno (1989). Some of the H_2 appears to be participating in a high-velocity flow into or out of the nucleus that is not shared by the ionized component of the gas.

This research has made use of the NASA/IPAC extragalactic database (NED) which is operated by the Jet Propulsion Laboratory, Caltech, under contract with the National Aeronautics and Space Administration. NSO/Kitt Peak FTS data used here were produced by NSF/NOAO. The authors would like to thank J. H. Black, R. C. Kennicutt, H.-W. Rix, and L. M. Shier for useful discussions. We also wish to thank the anonymous referee whose comments improved this paper. This research was funded by grant AST 91-16442 from the National Science Foundation.

REFERENCES

Aaronson, M. 1977, Ph.D. thesis, Harvard Univ.
Bekki, K. 1995, MNRAS, 276, 9
Black, J. H., & van Dishoek, E. F. 1987, ApJ, 322, 412
Campins, H., Rieke, G. H., & Lebofsky, M. J. 1985, AJ, 90, 896
Clegg, R. E. S. 1987, MNRAS, 229, 31P
Condon, J. J., & Yin, Q. F. 1990, ApJ, 357, 97
Devereux, N. A., Becklin, E. E., & Scoville, N. A. 1987, ApJ, 312, 529
Draine, B. T., & Roberge, W. G. 1982, ApJ, 259, L91
Elmegreen, B. V. G., Meloy Elmegreen, D., & Montenegro, L. 1992, ApJS, 79, 37
Engargiola, G. 1991, ApJS, 76, 875
Frogel, J. A., Persson, S. E., Aaronson, M., & Mathews, K. 1978, ApJ, 220, 75
Frogel, J. A., & Whitford, A. E. 1987, ApJ, 320, 199
Goldader, J. D., Joseph, R. D., Doyon, R., & Sanders, D. B. 1995, ApJ, 444, 97
Ho, P. T. P., Beck, S. C., & Turner, J. L. 1990, ApJ, 349, 57
Hollenbach, D. J., & Shull, J. M. 1977, ApJ, 216, 419
Huang, Z. P., Thuan, T. X., Chevalier, R. A., Condon, J. J, & Yin, Q. F. 1994, ApJ, 424, 114
Hudgins, D., Herter, T., & Joyce, R. J. 1990, ApJ, 354, 57
Hummer, D. G., & Storey, P. J. 1987, MNRAS, 224, 801
Ishizuki, S., Kawabe, R., Ishiguro, M., Okumura, S. K., Morita, K.-I., Chikada, Y., Kasuga, T., & Doi, M. 1990, ApJ, 355, 436
Kleinmann, S. G., & Hall, D. N. B. 1985, ApJS, 62, 501
Krabbe, A., Sternberg, A., & Genzel, R. 1994, ApJ, 425, 72
Latter, W. B., Hora, J. L., Kelly, D. M., Deutsch, L. K., & Maloney, P. R. 1993, AJ, 106, 260
Lebofsky, M. J., & Rieke, G. H. 1979, ApJ, 229, 111
Livingston, W., & Wallace, L. 1991, NSO Tech. Rep. 91-001 (Tucson: NOAO)
Maeder, A. 1992, private communication
Maloney, P. R., & Black, J. H. 1988, ApJ, 325, 389
Maiolino, R., Rieke, G. H., & Rieke, M. J. 1996, AJ, in press
McLeod, K. K., Rieke, G. H., Rieke, M. J., & Kelly, D. M. 1993, ApJ, 412, 111
Moorwood, A. F. M., & Oliva, E. 1988, A&A, 203, 278
Nussbaumer, H., & Storey, P. J. 1988, A&A, 193, 327
Oliva, E., & Origlia, L. 1992, A&A, 254, 466
Origlia, L., Moorwood, A. F. M., & Oliva, E. 1993 A&A, 280, 536
Rieke, G. H. 1976, ApJ, 206 L15
Rieke, G. H., & Lebofsky, M. J. 1978, ApJ, 220, L37
———. 1985, ApJ, 288, 618
Rieke, G. H., Lebofsky, M. J., Thompson, R. I., Low, F. J., & Tokunaga, A. T. 1980, ApJ, 238, 24
Rieke, G. H., Loken, K., Rieke, M. J., & Tamblyn, P. 1993, ApJ, 412, 99 (RLRT93)
Rix, H.-W., Carleton, N. P., Rieke, G. H., & Rieke, M. J. 1990, ApJ, 412, 99
Roche, P. F., Aitken, D. K., Smith, C. H., & Ward, M. J. 1991, MNRAS, 248, 606
Rogstad, D. H., & Shostak, G. S. 1972, ApJ, 176, 315
Shields, J. C. 1993, ApJ, 419, 181
Shier, L. M. 1995, private communication
Shier, L. M., Rieke, M. J., & Rieke, G. H. 1994, ApJ, 433, L9
Sternberg, A., & Dalgarno, A. 1989, ApJ, 338, 197
Telesco, C. M., Dressel, L. L., & Wolstencroft, W. D. 1993, ApJ, 414, 120
Tenjes, P., Haud, U., & Einasto, J. 1994, A&A, 286, 753
Thronson, H. A., & Greenhouse, M. A. 1988, ApJ, 327, 671
Tremaine, S., Richstone, D. O., Byun, Y., Dressler, A., Faber, S. M., Grillmair, C., Kormendy, J., & Lauer, T. R. 1994, AJ, 107, 634
Tully, R. 1988, Nearby Galaxies Catalog (Cambridge: Cambridge Univ. Press)
Turner, J. L., & Ho, P. T. P. 1983, ApJ, 268, L79
Vanzi, L., Rieke, G. H., Rieke, M. J., & Engelbracht, C. W. 1996, in preparation
Williams, D. M., Thompson, C. L., Rieke, G. H., & Montgomery, E. F. 1993, Proc. SPIE, 1946, 482
Witt, A. N., Thronson, H. A., & Capuano, J. M. 1992, ApJ, 393, 611
Wade, K., & Habe, A. 1992, MNRAS, 258, 82